Biosensors and Bioelectronics 202 (2022) 114010

Contents lists available at ScienceDirect

Biosensors and Bioelectronics

journal homepage: www.elsevier.com/locate/bios

Multielectrode biosensor chip for spatial resolution screening of 3D cell models based on microcavity arrays

Franziska D. Zitzmann [a,1], Sabine Schmidt [a,1], Max Naumann [a], Detlev Belder [b], Heinz-Georg Jahnke [a,*], Andrea A. Robitzki [a,c]

[a] Center for Biotechnology and Biomedicine, Molecular Biological-biochemical Processing Technology, Leipzig University, Deutscher Platz 5, D-04103, Leipzig, Germany
[b] Institute of Analytical Chemistry, Leipzig University, Linnéstraße 3, 04103, Leipzig, Germany
[c] Karlsruher Institute of Technology (KIT), Hermann-von-Helmholtz-Platz 1, 76344, Eggenstein-Leopoldshafen, Germany

ARTICLE INFO

Keywords:
Selective laser etching
Microcavity array technology
Electrochemical impedance spectroscopy
3D cell culture
MDA-MB-231
Field potential recording

ABSTRACT

Three-dimensional cell models represent the native in vivo situation more closely than two-dimensional cultures and are therefore preferred today for in vitro studies. In this context, there is a great demand for fast, non-invasive, real-time, and label-free methods that are capable for detailed analyses of three-dimensional cultures. To characterize heterogeneous cultures or to detect localized drug effects, a measurement method such as impedance spectroscopy in combination with microcavity arrays (MCAs) is desirable, which additionally offers spatial resolution. To overcome these limitations of the previously described MCA based on opaque silicon substrates and a square shape with four measurement electrodes imposed by the crystal structure, we used the selective laser etching (SLE) method to fabricate microcavities in fused silica and borosilicate glass without geometric constraints. We successfully developed MCAs with variable base including up to eight measurement electrodes in one cavity, which allows the increase in the number of electrode combinations to improve spatial resolution. In addition, we integrated a central cone electrode at the cavity bottom to extend the spatial resolution on the z-axis. To demonstrate the capability of the MCAs, we used MDA-HB-231 spheroids with an enclosed glass sphere to show that the heterogeneity of the model is evident in the relative impedance spectra. Analyses on various cell spheroids highlight the broad applicability of glass MCAs. In conclusion, our SLE-fabricated MCA clearly improve bioelectronic analyses of cellular changes in heterogeneous 3D models. Thus, bioelectronic analysis of electrophysiologically active cells and tumor biopsy samples could significantly benefit from our development.

1. Introduction

Due to the fact that three-dimensional cell culture models represent the native in vivo situation more precisely than 2D cultures, they offer a real-time strategy for the development of a rapid and biomimetic system for predicting, monitoring, and diagnosing the drug effects. By using multicellular model systems, complex tissue-like 3D constructs can be generated to mimic the properties and functions of native tissues due to their heterogeneity. Even through so-called organ-on-a-chip platforms, physiological environments are simulated by dynamic fluid flows or forces (Azizipour et al., 2020). Thus, 3D cell models lead to the formation of adequate cell-cell and cell-matrix contacts, which are critical for signal transduction and cellular communication regulating fundamental processes such as growth, proliferation, differentiation, migration, and programmed cell death (Li and Lee, 2020). For the aforementioned reasons, 3D cell models in particular are suitable for cell studies with regard to future clinical applications as well, and continuously improving methods are developing for the generation of in vivo-like 3D cell models (Augustine et al., 2021).

In this context, the development of fast, non-invasive, real-time, and label-free analysis technologies for 3D cultures is essential to provide detailed non-destructive information about three-dimensional cultures (Gerasimenko et al., 2020; Schmid et al., 2016). Especially for the characterization of heterogeneous 3D cultures or to detect the localized drug effect in 3D cultures, measurement techniques with high spatial resolution are in demand. For this purpose, several studies have been

* Corresponding author.
E-mail address: heinz-georg.jahnke@bbz.uni-leipzig.de (H.-G. Jahnke).
[1] These authors contributed equally to this work.

https://doi.org/10.1016/j.bios.2022.114010
Received 25 October 2021; Received in revised form 24 December 2021; Accepted 14 January 2022
Available online 19 January 2022

described in the literature that investigated the heterogeneity of, for example 3D tumor models using quantitative spatial cell metabolism studies (Heaster et al., 2019), long-term live imaging and multiscale analyses with fluorescently labeled organoids (Hof et al., 2021), or by developed quantitative image analysis tools based on fixed tumor spheroids (Allenby et al., 2017). A very suitable technique is impedance spectroscopy in combination with microcavity arrays (MCA), which offers the advantage of non-invasive monitoring of a long-term culture in a high-throughput screening (Chiappalone et al., 2003), providing information about changes in morphology (Szulcek et al., 2014), drug penetration and the effect of cytotoxic or bioactive molecules (Jahnke et al., 2014) with regard to electrophysiological properties of neuronal cells (Bagnaninchi and Drummond, 2011) and cardiomyocytes (Lopez et al., 2018). In this context, MCAs based on opaque silicon substrates have been developed to analyze three-dimensional cell cultures bioelectronically (Kloß et al., 2008), which comprises four measuring electrodes in one plane and their potential for functional drug screening has been demonstrated in various studies (Fleischer et al., 2019; Kloss et al., 2008; Seidel et al., 2019). A novel work uses the same approach but only provide two electrodes per cavity (Pan et al., 2020). However, the analysis of 3D models such as tumor organoids requires a biosensor with higher resolution to detect localized drug effects in 3D cultures due to complex culture heterogeneity (Nii et al., 2020).

The silicon crystal structure limits the geometry of the etched microcavities to a square shape with an angle of 54.7° (Gos lvez and Nieminen 2003; Kloß et al., 2008). Therefore, increasing the number of measurement electrodes with this type of MCA is not an option, the spatial resolution of the biosensor for complex analysis cannot be increased. An alternative fabrication method for microcavities is the newly developed selective laser etching (SLE) process, which can be used to fabricate precise microstructures in glass (Butkutė et al., 2021; Kim et al., 2019). Therefore, the aim of the present study was to develop a MCA-based biosensor in glass using the SLE technique in order to improve the bioelectronic analysis of heterogeneous 3D cell cultures. To increase the MCA measurement resolution, microcavities were fabricated with modified shapes aiming for additional measuring electrodes.

Thus, in the present work, MCAs fabricated in fused silica and borosilicate glass with up to eight measurement electrodes in one plane and an additional electrode on a central cone structure in the center of the cavity bottom in a second plane are presented and shown that the novel microcavities significantly increase the spatial resolution of analyses of heterogeneous 3D objects by the additional measuring electrodes. Especially with regard to the analysis of 3D cell samples, which inherently exhibit extreme heterogeneity such as primary tumors (Dagogo-Jack and Shaw, 2018) or mesenchymal stem cells for clinical applications (Costa et al., 2021), this increase in spatial resolution in particular offers a decisive advantage in their analysis. In addition, this MCA chip is designed to be adaptable to additional cavity sizes and can easily integrate into microfluidic systems due to the transparent properties of glass.

2. Material and Methods

2.1. Microcavity fabrication

The microcavities were designed as an inverted frustum of a pyramid with a height equal to 2/3 of the side length of 400 μm with a square, hexagonal or octagonal base area. Microcavities with five electrodes consist of a quadratic area as basic geometric shape and a cone at the bottom of the cavity (Fig. S1). The electrodes of all cavity shapes were designed as described in the supplementary part.

The microcavities were fabricated in borosilicate (BS) and fused silica (FS) glass using the selective laser-induced etching (SLE) process. An ultrashort pulsed laser is used to pre-pattern the layout designed in CAD. Due to the significantly higher etch rate of the laser-treated areas compared to the untreated areas of the glass, complex three-dimensional structures can be directly applied to the glass (Gottmann et al., 2017; Hermans, 2014).

The cavity layouts were designed using Autodesk Inventor Professional 2018 CAD software (San Rafael, CA, USA) and converted to machine code using Alphacam 2017 R2 CAM software (Vero Software GmbH, Neu-Isenburg, Germany). Subsequently, the glass substrates (MicroChemicals GmbH, Germany) were placed on a xy-linear translation unit inside the SLE device (FEMTOprint f200aHead 2 PP) and processed with a 1030 nm Yb: YAG laser (pulse energy: FS 230 nJ, BS 600 nJ; pulse length: 400 fs). Afterwards, the processed fused silica substrates were etched in KOH solution (45 wt%, 84 °C) in a pulsed ultrasonic bath, and the borosilicate glass substrates were etched with HF solution (10 wt%; room temperature). To structure the microcavities, the electrodes are fabricated using a lift-off process which is explained in detail in the supplementary part. Finally, a reservoir for medium is placed on the surface.

2.2. Bioelectronic analysis of 3D models

The bioelectronics analysis were done as previous described (Fleischer et al., 2019). Briefly, impedance spectra were recorded with an Agilent 4294A (Agilent Technologies, USA) (500 Hz–5 MHz, 51 measurement points, +-10 mV amplitude) and a self-developed software (IMATadvanced). Field potentials were recorded with a sampling rate of 4 kHz for 15 min using a MEA1060BC amplifier system (Multichannel Systems, Germany). Action potentials and amplitude (contraction rate analysis) were analyzed with a self-developed software (FiPRAT).

2.3. Data analysis

Impedance signal spectra and maximum amplitude of the measured objects (relative impedance) were calculated from impedance magnitude spectra by a self-developed software (IDAT v3.7) according to $|Z|\,\mathrm{rel}\,(\%) = ((|Z|\mathrm{sphere} - |Z|\mathrm{blank})/|Z|\mathrm{blank} \times 100)$ and determines its maximum.

For analysis of the impedimetric resolution, the measured maximum impedances between electrodes (E) were divided into groups (G) depending on the distance between the electrodes (4E/2G; 8E/4G; 5E/3G). Subsequently, the significance of the impedance values was determined in relation to the group median and was converted into a line width. Non-significant impedance differences to the median were shown as dashed lines. Impedance differences greater than or equal to 15 were defined as maximum line width. For MCAs with a cone, the median of the measurements where the glass sphere was farthest or closest to the cone electrode was chosen as the minimum or maximum value for evaluating the impedance resolution. No upper limit was defined and the differences were again converted to line widths.

For statistical analyses GraphPad Prism 5 (GraphPad Software, USA) was used. Significance analyses were performed using ANOVA and Bonferroni post hoc test. Differences between two means with $p < 0.05$ were considered significant (*), $p < 0.01$ very significant (**), and $p < 0.001$ highly significant (***).

2.4. Cell culture

Breast cancer cells MDA-MB-231 (ATCC, USA) were cultivated in RPMI1640 supplemented with 10% fetal bovine serum, antibiotics (2U/mL penicillin, 0.2 μg/mL streptomycin, 20 μg/mL gentamycin), and 2 mM GlutaMAX (all from Life Technologies, Germany). A modified hanging drop method was used to generate hybrid spheroids, as detailed in Fig. S2. Briefly, glass spheres (BioSpec, USA, diameter: 0.1 mm) were pipetted onto the top of Petri dishs in 1 xPBS drops and 5000 cells were seeded onto it in 25 μL medium. The closed Petri dishes were cultured for 4 days. Finally, the spheroids were transferred to non-adherent 96 well plates with U-bottom (Greiner Bio-One, Germany). All cell cultures were maintained at 37 °C and 5% CO_2.

3. Results and Discussion

3.1. MCAs fabricated in glass have a higher impedimetric sensitivity

To improve microcavity-based 3D culture analysis with respect to bioelectronic and photonic measurement techniques, we used SLE to fabricate novel microcavity structures in glass. In this context, we tested the fabrication in fused silica (FS) and borosilicate (BS) with the aim to identify the difference between these glass types and their suitability for the microcavity fabrication (Fig. 1). Exemplarily, MCAs were fabricated containing twelve individual square microcavities with a uniform diameter of 400 μm and a depth of 188 μm. Each cell chamber contained three microcavities and a semicircular counter electrode for field potential recordings (Fig. 1E).

SEM analysis demonstrates that square microcavities can be very precisely structured in both glass types using the SLE technique (Fig. 1A). Additionally, the etched surfaces of FS appeared to be significantly smoother than those of BS. A further analysis of the surface roughness confirmed this (Fig. S3). Images captured by confocal microscopy demonstrate no difference in the lateral resolution of the structure between the two materials. Nevertheless, it can be observed that the etched surface of the BS substrates is rougher than the surface of FS substrates due to the increased light scattering. The determined roughness values, which were one decade higher for BF, indicated this as well (Fig. S3). In this case, the reason for the difference is the varying composition of the glasses and the associated variations in the etching processes (Bischof et al., 2021; Hermans, 2014; Jin et al., 2013).

Gold electrodes (0.006 mm^2 electrode area each) were placed on the four side walls of the cavity to analyze cellular parameters by impedance and record extracellular field potentials. In order to be able to fabricate cavities with additional electrodes in a further development step, a semicircular electrode shape was selected. That the electrode shape had

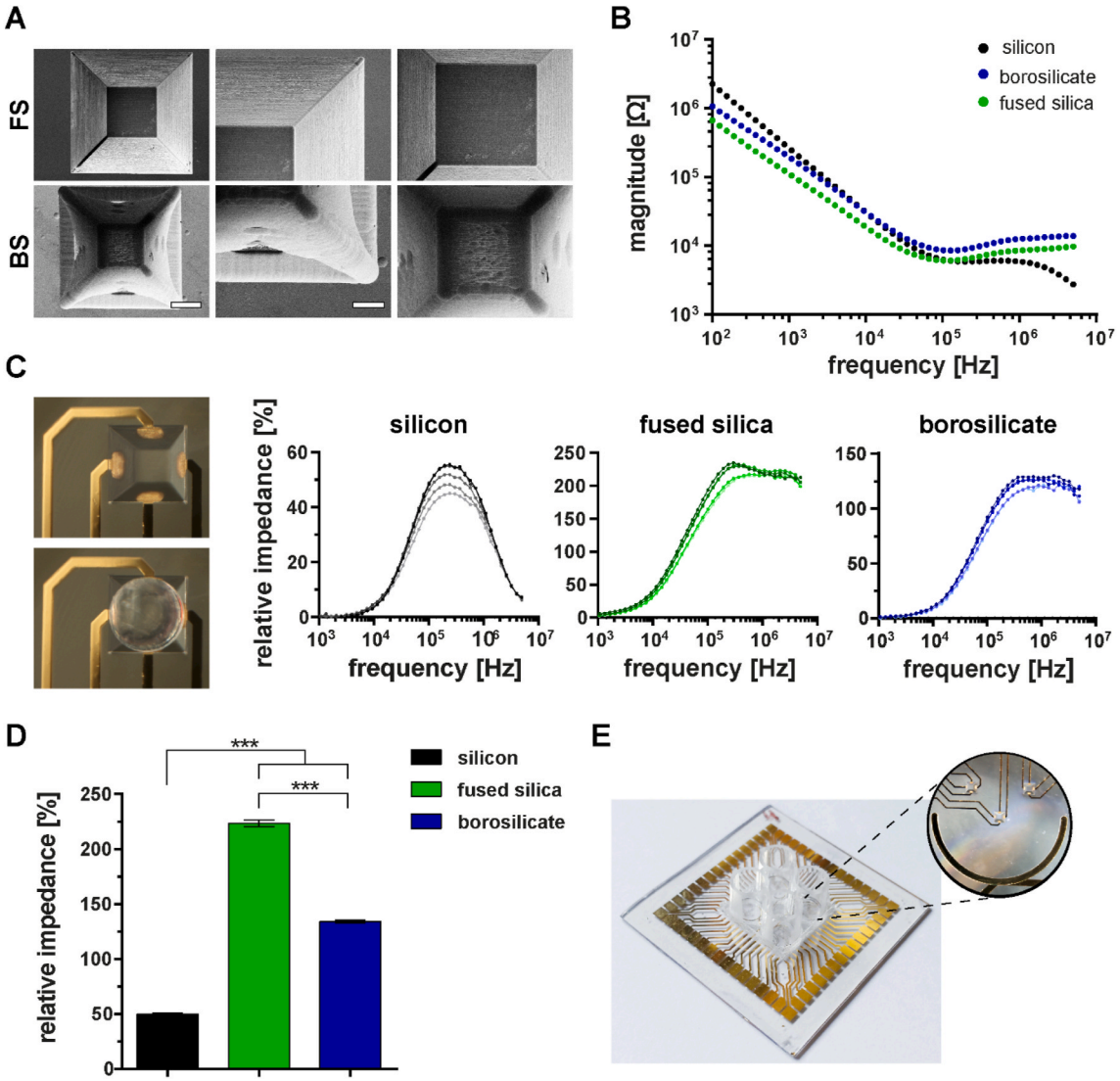

Fig. 1. Microcavity arrays with square base area fabricated by SLE in fused silica and borosilicate glass. (A) SEM images of the square cavities (400 × 400 μm) in fused silica glass (FS) and borosilicate glass (BS) with enlarged images of the cavity walls (center) and cavity bottoms (right, scale bar: 100 μm, magnification: 50 μm). (B) Comparisons of impedance magnitude spectra in the frequency range of 100 Hz to 10 MHz (mean, n ≥ 3 cavities with 6 spectra each). (C) Impedimetric characterization of the microcavity arrays by analysis of the relative impedance of glass spheres as an ideal model. Shown are light microscopic images of an empty microcavity and one with a positioned glass sphere as well as the relative impedance spectra exemplarily of five glass spheres in the size range of 400–425 μm (mean, n = 3 measurements per sphere with 6 spectra each). (D) Statistical analysis of the maximum relative impedance of five glass spheres measured in the three different microcavity arrays (mean ± SEM, n ≥ 3 cavities with 6 spectra each and three measurement replicates). (E) Image of the multielectrode microcavity chip fabricated in fused silica with four attached cell chambers. Detailed image shows a chamber with three measuring cavities and a semicircular counter electrode for multiparametric analyses.

no influence on the magnitude spectra of the microcavities at constant area is shown in Fig. S4. The semicircular electrode shape was compared with a rectangular, which is present in the silicon MCA. Consequently, MCAs fabricated in different materials with the same electrode area can be compared due to the independence of the electrode geometry. In a further analysis, we investigated the long-term stability of the electrodes it was shown that the use of the MCAs for biological analyses does not lead to a change in the magnitude spectra of the measuring electrodes over the period investigated (Fig. S5). The fabricated microcavities have a high stability and are therefore suitable for long-term studies.

The MCAs made of glass were comparatively impedimetrically analyzed for characterization with the MCA based on silicon substrates (400 μm diameter cavities were used, Fig. 1). A direct comparison of the MCAs under identical measurement conditions is possible. The cell-free impedance magnitude spectra of the microcavities are comparable for both glass types. In the frequency range from 500 Hz to 20 kHz, the spectrum of silicon MCA is similar to the glass ones, but differs significantly in the higher frequencies. The microcavities made of the semiconductor material silicon show a significant signal loss in the higher frequency range which means that they have a higher parasitic capacitance due to the different substrate material and structure.

The obvious advantage of glass MCAs is their optical transparency (Fig. 1C). For direct comparison of the relative impedance of the three MCA types, glass spheres were chosen as an ideal model. The glass spheres do not change within the individual measurements and thus a comparison of the MCAs is possible. Glass spheres with a diameter of 400–460 μm are suitable for the designed cavity size. Further sizes can be analyzed straightforwardly by adjusting the microcavity design.

As a unit, 5 glass spheres in microcavities of the three materials were measured and their relative impedance spectra were shown. Although the glass spheres were very similar, the spectra of the individual spheres showed differences. Additionally, the course of the spectra of silicon microcavities and the two glass types show significant variations. The spectra of silicon had a Gaussian shape with a maximum at 2 kHz. In contrast, the spectra of glass MCAs showed a maximum at 2 kHZ as well, but a plateau is observed in the further course. As already seen in the magnitude spectra, biological information are included in the higher frequency region and is not truncated as in silicon MCAs. That relative impedance spectra can provide biological information about the structure of 3D spheroids and their proportion of extracellular spaces even in the 5-MHz range has already been shown in early impedimetric studies and correlated with an equivalent circuit (Jahnke et al., 2014). Therefore, glass MCAs offer high potential for further analysis of 3D cell models such as tumor fragments and their metastases. To compare the maximum relative impedance of MCAs, the same glass spheres were analyzed in microcavities ($n \geq 3$ cavities with 5 spheres each, Fig. 1D). The results show that the lowest impedance was obtained with silicon MCAs (49.58 ± 1.54%), while FS MCAs had the highest (223.41 ± 2.89%), followed by BS MCAs (133.97 ± 1.21%).

In summary, higher maximum relative impedances can be determined with the new glass MCAs, resulting in a 4.5-fold higher signal amplitude for FS MCAs and 2.7-fold higher signal amplitude for BS MCAs in comparison to silicon MCAs. The difference in maximum relative impedance between FS and BS is assumed to be due to the rougher surface of the BS sidewalls and the resulting degraded contact area of the sphere on the electrodes (cf. Fig. 1A, Fig. S3).

3.2. The SLE process enables cavity forms for additional measuring electrodes

Compared to the fabrication of silicon-based MCAs, the SLE-based fabrication of microcavities has no geometrical restrictions (angles, structure, depths) (Butkutė et al., 2021; Kloß et al., 2008). Therefore, we were able to fabricate microcavities with new geometries to increase the electrode number by adding additional side walls and a central cone at the bottom of the cavity. In addition to the square base, microcavities with hexagonal or octagonal bases were designed. The cone structure was inserted for microcavities with a square base.

The additional measuring electrodes significantly increase the three-dimensional resolution of the bioelectronic analysis. The more electrodes there are in a microcavity, the more spectra of electrode pairs can be impedimetrically analyzed and consequently the spatial resolution of dielectric properties could be increased. For cavities with six or eight electrodes, the resolution is increased in one measuring plane, whereas in the case of the cavity design with cone, even a three-dimensional analysis is theoretically possible (Fig. S6).

3.2.1. Microcavities with up to eight electrodes for analysis in one plane

In order to analyze 3D objects in a higher resolution, the square microcavities were extended and fabricated with hexagonal or octagonal bases (Fig. 2). The SEM analysis showed that there are no restrictions in geometry shapes with the SLE method. The difference between the two types of glass is again evident in the images, as again the walls of the FS cavities seem much smoother than those of BS (Fig. 2A). A gold electrode with an electrode area of 0.006 mm^2 (same as square microcavities) was placed on each sidewall (Fig. 2B).

To directly compare the microcavities, the maximum relative impedance was again measured using glass spheres as an ideal model (Fig. 2C). The analysis demonstrated that the values determined in each case were in the same range as for the square base microcavities. A maximum relative impedance of 188.1 ± 1.25% was determined for hexagonal cavities made of FS and 208.6 ± 3.23% for octagonal cavities. In contrast, the values for BS microcavities were lower (hexagonal: 161.4 ± 2.28%, octagonal: 127.9 ± 0.55%), as already observed for the square microcavities. The corresponding magnitude spectra and relative impedance spectra of the different microcavities were shown in Fig. S6.

Based on the 3D height profile, exemplified by a microcavity with hexagonal base, it is clearly seen that the passivation layer is thinner towards the edge of the cavity than further away (Fig. S8). This is a result of the softlitographic process using SU-8 resist and indicates that there can be an increase in electrode area due to the lack of passivation at the edge.

3.2.2. A measuring electrode on the cavity bottom can extend the impedimetric analysis in the third dimension

The innovative SLE process not only allows a modified cavity shape, but also enables a central cone structure at the bottom. This was selected in the form of a circular cone, which allows a circular electrode (same area as sidewall electrodes) to be used for the analysis of round three-dimensional 3D objects. To prove the principle, a square electrode shape was taken as a basis.

SEM analysis showed that both FS and BS can be used to fabricate microcavities with a cone (Fig. 3A). The cone structure for the fifth measuring electrode was fabricated more accurately in FS. The surface of the cone made in borosilicate, on the other hand, appears rather irregular, resulting in a significantly enlarged surface area.

For contacting the cone electrode, the conductive path was selected to be placed over the corner edge of the cavity (Fig. S10). Thus, the maximum distance to the sidewall electrodes could be achieved. To characterize the microcavities with cones made of both glass types, the impedance was measured in the frequency range from 100 Hz to 5 MHz in the cell-free state and the magnitude spectra were shown in Fig. S10. The spectra between the cone electrode and the electrodes on the side walls had a lower level than the spectra between the side wall electrodes. This effect was significantly more noticeable for microcavities made of borosilicate glass. The reason of the lower spectra of the cone electrode is probably that the area of the electrode was increased as a result of incomplete passivation of the conductive path at the edge of the electrode, thereby reducing the self-impedance of the cone electrode. For passivation, the photoresist SU-8 was used in a thick resist process. The technique is very suitable for passivation of conducting paths on the glass surface in 2D (Seidel et al., 2019; Zhang et al., 2010). However, it

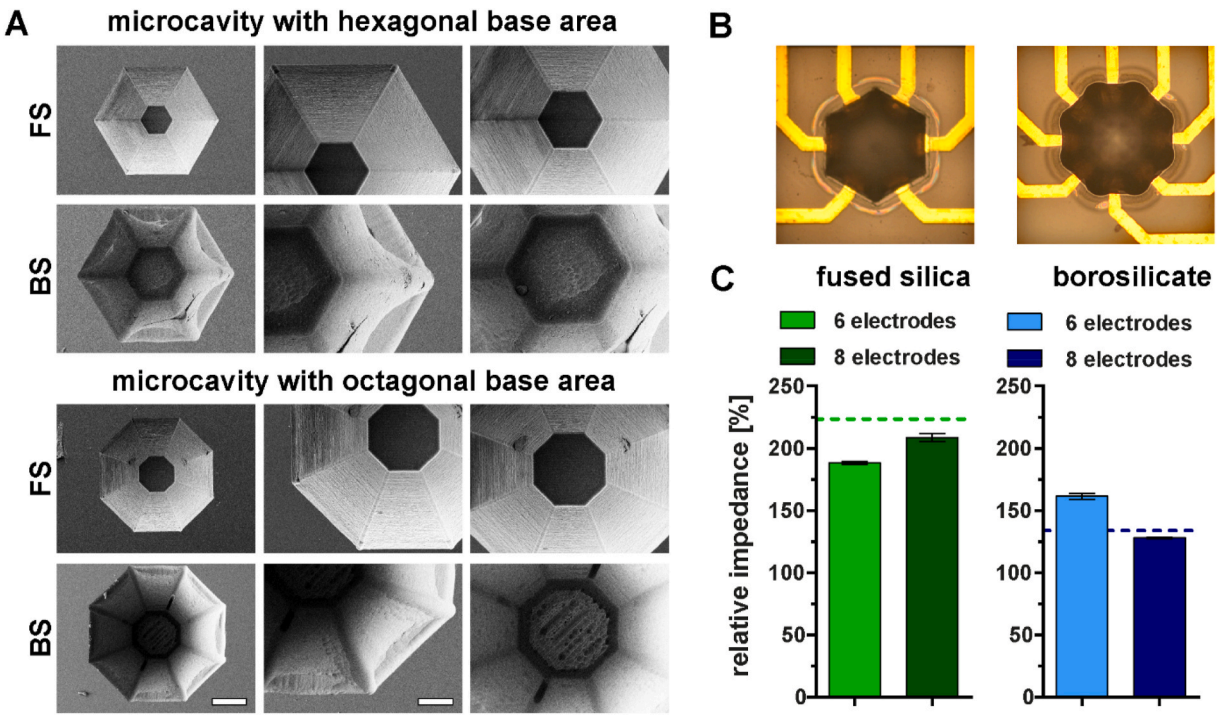

Fig. 2. Enhancement of measuring electrodes in microcavities by hexagonal and octagonal base areas. (A) SEM images of the cavities (400 × 400 μm) in fused silica glass (FS) and borosilicate glass (BS) with enlarged images of the cavity walls (center) and cavity bottoms (right, scale bar: 100 μm, magnification: 50 μm). (B) Light microscopic images of the structured cavities with six electrodes (left) and eight electrodes (right). (C) Statistical analysis of the maximum relative impedance of five glass spheres as an ideal model system (mean ± SEM, n = 5 cavities with 15 spectra each for microcavities with 6 electrodes or 28 spectra each for microcavities with eight electrodes; three measurement replicates each; dashed line represents maximum relative impedance of glass spheres in square cavities).

reaches its limits in passivating conducting paths in 3D, which run across the cavity with different side angles and height differences. The different areas in the cavity require dissimilar development times, which cannot be achieved with the one-step process, resulting in exposed areas of the conductive path. Since no more effective process is currently known, the used method is the best option for passivation of the cone electrode. To determine an optimal cone design, various cone structures were created based on a construction using AutoCAD, which differed in height and incidence angle of the cone (Fig. S6, image of microcavity with cone). It was found that the cone height for 3D cell models with a diameter of 400 μm and a cavity size of 400 μm is approximately 50–60 μm. For analyzing the maximum achievable measurement object signal, we used glass spheres once again to determine their relative impedance. The resulting spectra were divided into three groups (opposite electrodes, across the corner, and to the cone) and averaged (Fig. S11). The results of all groups must be considered to determine the optimum cone structure for the following reasons. If the distance between the cone electrode and the glass sphere is too far and the glass sphere does not contact the electrode surface, the resulting relative impedance values are lower than when the glass sphere is in contact. However, if the cone structure is too high, the sphere will be in contact with the cone electrode, but the sphere will protrude beyond the cavity and there will be no contact to the side electrodes. The relative impedance values of the side electrodes would therefore be low. Taking these points into account, it was found that for FS a cone structure with a height of 50 μm, an angle of 20° for the cone structure and 35° for the cavity (Fig. S1) was optimal (corresponding to structure III in Fig. S11). The same parameters were determined for BS microcavities, except for the height of the cone, where an optimum height of 60 μm was determined (corresponding to structure IV).

A comparison of the relative impedance spectra of glass microcavities initially shows the same pattern in both cases as for square microcavities without cones (Fig. 3B). A maximum is observed at about 5 kHz, followed by a plateau phase in the high-frequency region. This means that the spectra measured between the cone electrode and the sidewall electrodes contain also information in the high frequency range and are suitable for further analysis of cell models. However, there is a significant difference in the spectra height to the cone and between the others, which confirmed the statistical analysis (Fig. 3C). The analysis was also performed for direct comparison with a group of identical glass spheres. The highest values were obtained between opposite electrodes (FS: 173.5 ± 7.78%; BF: 70.48 ± 1.89%). The maximum relative impedances measured across the corners were slightly lower, 159 ± 6.71% for FS microcavities and 66.82 ± 1.85% for BS ones. The reason for this effect is suggested by the measurement arrangement, whereby the electric field can bypass the measured object to a larger extent through the medium. This results in a sum signal and causes lower maximum relative impedances. The lowest maximum relative impedances of the spheres were measured to the cone (FS: 104.1 ± 2.08%, BS: 40.08 ± 1.08%). As described above, the reason for this is the lower intrinsic impedance of the microcavities, which results manufacturing-related from an enlarged electrode area of the cone electrode. Structuring and the associated passivation in 3D objects with height differences of several 100 μm is very challenging. The further development of existing structuring techniques is therefore a task for the future.

Overall, all maximum relative impedances of the microcavities with cone of fused silica were higher than those of microcavities made in borosilicate glass. Even though the impedance values between the cone electrode and the side electrodes are much lower than those of the sidewall electrodes, the impedance values are higher compared to the silicon MCAs and the frequency spectrum is still not cut off after 5 kHz.

3.3. Increasing the number of measurement electrodes in MCAs leads to higher spatial resolution in impedance analyses of heterogeneous 3D models

A higher number of measuring electrodes distributed around a 3D object theoretically leads to an increased spatial resolution. This is of

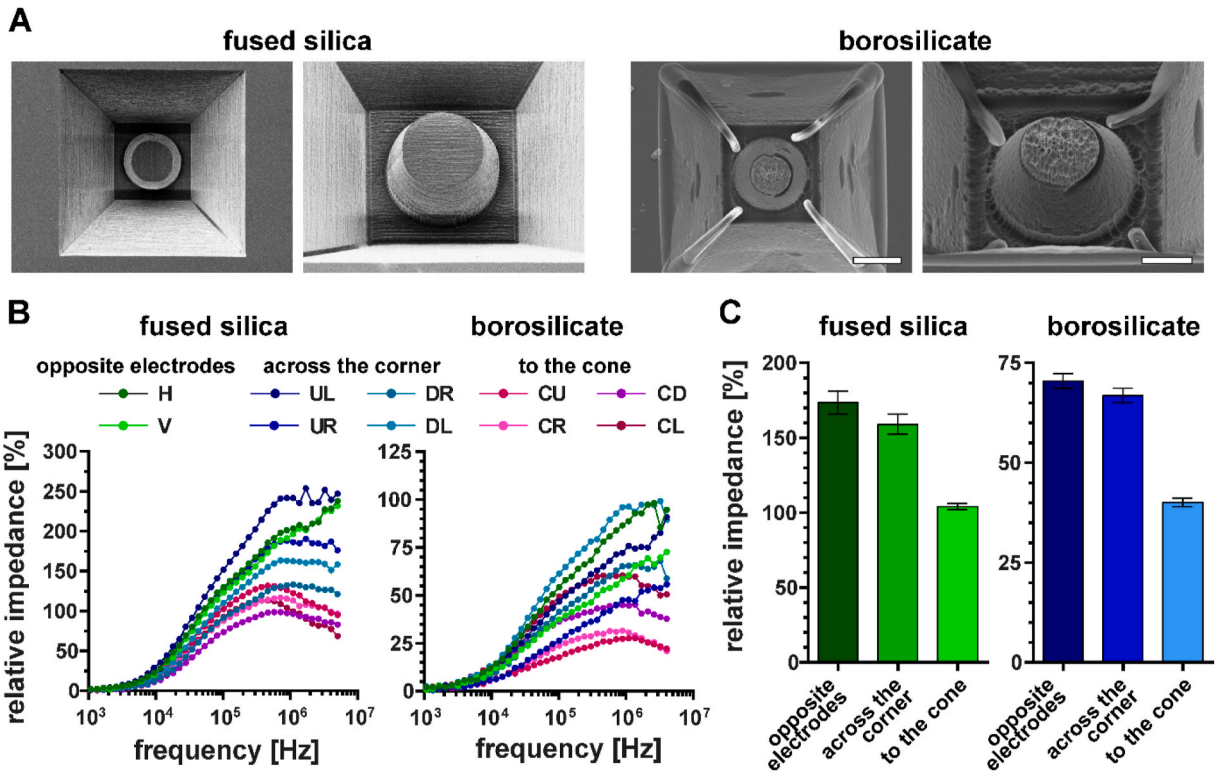

Fig. 3. Extension of spatial resolution in impedance analyses by additional measuring electrode on cone structure at the bottom of the microcavity. (A) SEM images of the square cavities and cone for lower electrode in fused silica glass and borosilicate glass with enlarged images of the cavity bottom (inclination: 30°,scale bar: 100 μm, magnification: 50 μm). (B) Relative impedance spectra of the microcavities in the frequency range of 100 Hz to 10 MHz exemplarily for a measurement with a glass sphere as ideal model system. Shown are the 10 measured spectra grouped into the measurement directions opposite electrodes (H: horizontal, V: vertical), across the corner (electrode designation: U: upper, L: left, R: right, D: down) and to the cone (C: cone). (C) Statistical analysis of the maximum relative impedance of glass spheres measured in fused silica and borosilicate microcavities and grouped in the three measurement directions (mean ± SEM, n = 6 spheres with three measurement replicates each and previously the individual spectra of the different measurement directions were averaged: opposite electrodes: H/V, across the corner: UL/UR/DR/DL, to the cone: CU/CD/CR/CL).

great interest for label-free analysis of heterogeneous 3D models e.g. with areas containing different cell types with varying biological properties, such as tumor tissue, differentiated stem cells, or organoid cultures. In order to verify if this is the case, a model system was chosen consisting of cellular spheroids including glass spheres. The aim was to create two regions within the spheroid that have clearly different dielectric properties and therefore, can be distinguished by impedimetric measurements. The melanoma cell line MDA-MB-231 was chosen because it generates stable spheroids of the required size of 300–500 μm in diameter, yet has a relatively low relative impedance (Froehlich et al., 2016; Huang et al., 2020; Jahnke et al., 2019). Thus, the impedance difference between the areas glass and cells should be clearly given. This was verified by comparatively measuring 3D models with the same diameter in microcavities impedimetrically (Fig. S11). Based on the relative impedance spectra, comparatively shown for pure MDA-MB-231 spheroids measured in all FS and the silicon MCA (Figs. S12A–C), the maximum relative impedances were determined and plotted for MCAs with octagonal base areas (Fig. S12D). MDA-MB-231 spheroids had a relative impedance of 41.41 ± 4.77%, while for glass spheres it was 139.1 ± 2.34%. Thus, glass exhibits significantly higher relative impedance than MDA-spheroids. Consequently, a hybrid spheroid consisting of a glass sphere in the cell spheroid should have a higher impedance than the pure cell spheroids but a lower impedance than glass spheroids, which could be verified with the determined relative impedance of 57.54 ± 3.23% (Fig. S12D). The values were determined from the mean value of all spectra (n = 28). A significant difference between the cell spheroids and the hybrid spheroids was already evident. Therefore, when looking at the individual measurement spectra, it should be recognizable in which orientation the hybrid spheroid was located in the measurement cavity. The prerequisite to achieve this was a hybrid spheroid whose glass sphere is not located centrally in the 3D model. This enables different positions of the spheroid in the microcavity. To achieve this, a modified hanging drop method was chosen (Fig. S2). The method was able to generate stable spheroids that had a round shape and permanently contained a 100 μm in diameter glass sphere inside (Fig. 4). Based on the averaged maximum relative impedances of all spectra, it was initially not possible to see in the results how the spheroid was located in the cavity. But by a separate analysis of the spectra it could be shown that the novel MCAs lead to a significant increase of the impedimetric resolution in one as well as in two planes. The glass sphere position in the spheroid can be detected in the measuring cavity (Fig. 4). Comparatively, the analysis was made in microcavities with four, eight, and five electrodes. For each analysis, the shown spheroid was placed in the measurement cavity in the respective position as indicated in the illustration above and three different positions were selected as examples. For square-base microcavities, the six impedance spectra recorded for each of the three positions shown indicated that although the area in which the glass sphere was located during the measurement could be determined when the impedance spectra were analyzed separately, the area of the region was relatively large (Fig. 4A). Thus, this results in a relatively low resolution for these microcavities. In contrast, using the MCA with eight measuring electrodes, the glass sphere's position in the spheroid in the measuring cavity was clearly visible in the determined impedance spectra (n = 28) of the individual electrodes (Fig. 4B). The highest maximum impedances were determined in all three positions shown in the areas where the sphere was located during the measurement. The cone electrode was used to show the position of the sphere in the cavity in a second plane

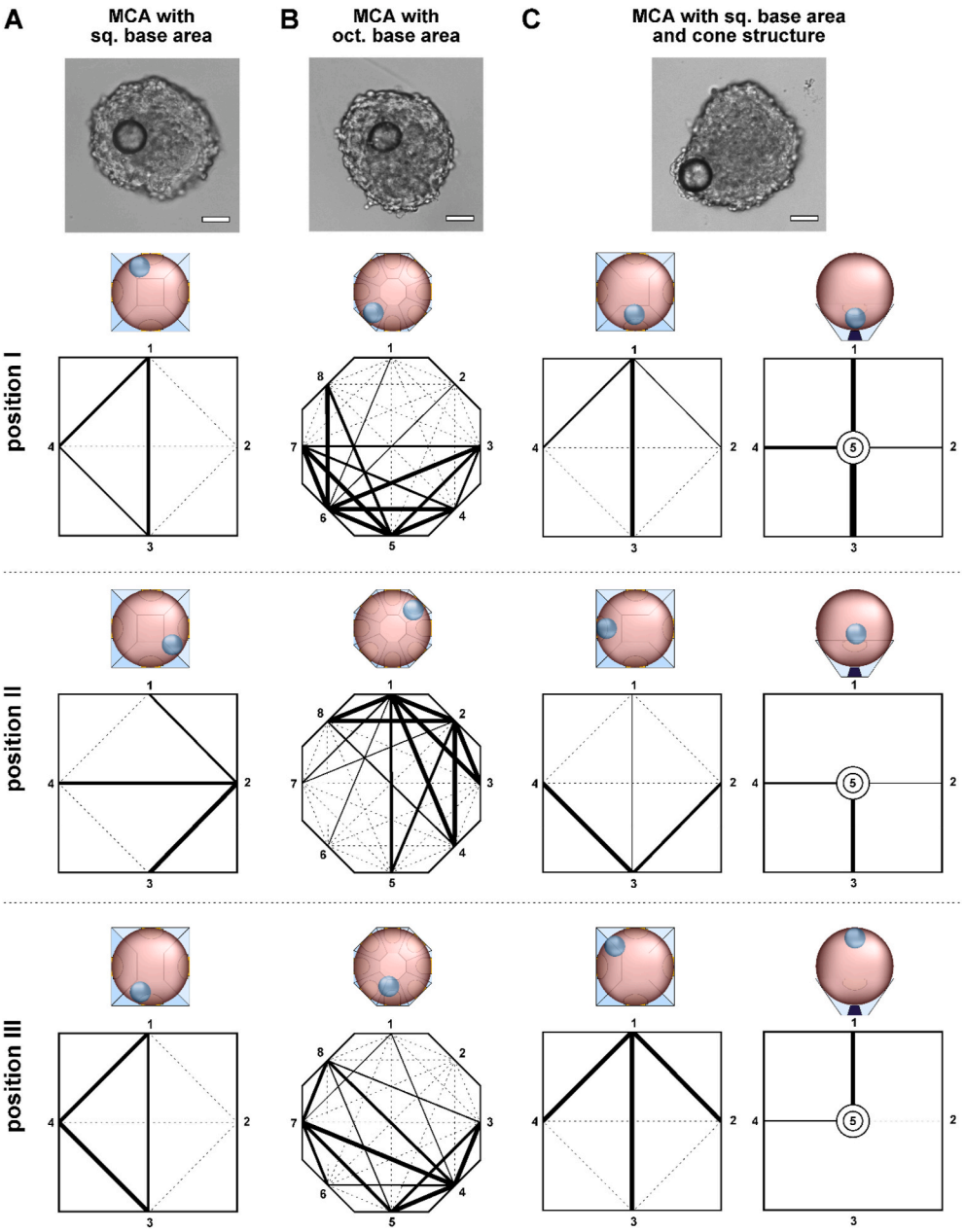

Fig. 4. Comparative analysis of impedimetric resolution of microcavities with various number of measuring electrodes in one and two planes using heterogeneous melanoma spheroids with enclosed glass spheres. The resolutions were analyzed in microcavities fabricated in fused silica with square base arena and four measurement electrodes (A), with octagonal base area and eight electrodes (B) and with square base area and cone for lower electrode with five electrodes in total (C). The maximum relative impedances of the MDA-MB-231 spheroids shown in phase contrast images were measured in three different positions (I-III) in the cavities. The variances of the measured values were converted into line widths and these were graphically displayed depending on the significance between the individual measuring electrodes (dashed lines = no significant increase in impedance). The locations of the spheroids with enclosed glass spheres in the measurement cavities are shown in each case in the images above (scale bar = 100 μm).

(Fig. 4C). The closer the sphere in the spheroid was to the cone electrode, the higher the relative impedance was due to the higher electrical resistance of glass in the equivalent circuit compared to cells (Seidel et al., 2016; Szulcek et al., 2014). Three positions were chosen with different proximity to the cone electrode (1st: on the electrode; 2nd: in the cavity center; 3rd: outside of the cavity). The measurement with the glass sphere closest to the electrode showed the largest region of significantly increased impedance, while the region of significantly increased impedance was lower at position II and lowest at position III. Despite the low intrinsic impedances of the cone electrode, these results could be measured (cf. Fig. 3), which proves the concept of the cone electrode. In summary, increasing the number of electrodes in both one plane (MCA with eight electrodes) and two planes (MCA with cone electrode) results in a significant enhancement of the impedimetric resolution.

To demonstrate the applicability of glass MCAs in different cell models, 3D cell models of three cell lines were impedimetrically analyzed in all four MCA types (Fig. S12). Here, the HT144 cell line represents a melanoma cell model, the LUHMES cell line a neuronal model, and the hCMCs derived from human stem cells a cardiac cell model. Both the heterogeneity and the structural differences of the 3D cell models are identifiable in this analysis.

The MCAs fabricated in glass additionally offer an excellent opportunity to study electrophysiological processes additionally to impedimetric analysis of electrophysiological active 3D models as shown, e.g., using cardiomyocyte clusters derived from human induced stem cells (hCMC, Fig. S14, movie S1). A group of five different hCMCs each were analyzed in MCAs with octagonal base and MCA with cone electrode with respect to impedance, frequency, and field potential parameters. Based on these analyses, it is shown that the novel MCAs are perfectly suited for multiparametric analysis with regard to parameters such as contraction rate, its amplitude, and a field potential-based detection of action potential duration (fAPD, not performed at this point) and could be used in a variety of studies.

Supplementary data related to this article can be found at https://doi.org/10.1016/j.bios.2022.114010.

4. Conclusion

In summary, we were able to demonstrate that SLE technology is a very suitable tool for fabricating microcavities in fused silica and borosilicate glass. Impedimetric characterization of the novel MCAs using glass spheres as an ideal model showed 4.5 times higher relative impedance for fused silica and 2.7 times higher for borosilicate compared to the silicon MCAs. In addition, the newly developed transparent MCAs have the distinct advantage that biological information of 3D models can be detected in the relative impedance spectra even in higher frequency ranges (>1 MHz). In order to insert additional measuring electrodes into microcavities, it was successfully demonstrated that the SLE technique enables the fabrication of microcavities with modified geometries for up to eight electrodes in one plane and a cone structure for three-dimensional analyses.

Using a heterogeneous spheroid model consisting of MDA-MB- 231 cells enclosing glass sphere, it was demonstrated that the electrode increase led to a significant increase in resolution and thus heterogeneous cell models in particular could be analyzed in more detail in further studies. Especially for electrophysiologically active 3D models such as cardiomyocyte cultures, the MCAs offer a great opportunity to perform multiparametric drug analyses, which could be demonstrated by first analyses with hCMCs with regards to impedance, frequency and field potential derivations.

In the present study, all analyses were performed using 400 μm diameter microcavities in a measurement setup with a maximum of 12 microcavities for parallel analysis. However, the SLE method and the adapted semicircular electrode shape allow individual adaptation of the cavity size to 3D cell models resulting in optimal bioelectronic analysis of 3D cell models of different sizes as well. In addition, the technique also offers the possibility for scaling up MCAs to standardized cultivation formats e.g. 96-well titer plate format for high-throughput applications. This would bring real-world applicability for e.g. drug development or clinical diagnostics much closer. Additonally, the glass microcavities offer the great opportunity of integration into microfluidic systems for an enhanced monitoring sensitivity of 3D cell models under hydrodynamic conditions, which will be further investigated in future studies.

Declaration of competing interest

The authors declare that they have no known competing financial interests or personal relationships that could have appeared to influence the work reported in this paper.

Acknowledgements

This work was funded by the German Research Foundation [grant number: DFG, 275695947]. The SLE device was funded by the Saxon Ministry of Science and the Fine Arts (SMWK) [project LasMino grant number: 100299999]. We thank Tobias Haensch and Valerie Thalhofer for cell culture assistance and Dr. Max Vollmering for his support with impedimetric resolution data analysis.

Appendix A. Supplementary data

Supplementary data to this article can be found online at https://doi.org/10.1016/j.bios.2022.114010.

References

Allenby, M.C., Misener, R., Panoskaltsis, N., Mantalaris, A., 2017. Tissue Eng. C Methods 23 (2), 108–117.
Augustine, R., Kalva, S.N., Ahmad, R., Zahid, A.A., Hasan, S., Nayeem, A., McClements, L., Hasan, A., 2021. Transl. Oncol. 14 (4), 101015.
Azizipour, N., Avazpour, R., Rosenzweig, D.H., Sawan, M., Ajji, A., 2020. Micromachines 11 (6), 599.
Bagnaninchi, P.O., Drummond, N., 2011. Proc. Natl. Acad. Sci. Unit. States Am. 108 (16), 6462–6467.
Bischof, D., Kahl, M., Michler, M., 2021. Opt. Mater. Express 11 (4), 1185–1195.
Butkutė, A., Baravykas, T., Stančikas, J., Tičkūnas, T., Vargalis, R., Paipulas, D., Sirutkaitis, V., Jonušauskas, L., 2021. Opt Express 29 (15), 23487–23499.
Chiappalone, M., Vato, A., Tedesco, M., Marcoli, M., Davide, F., Martinoia, S., 2003. Biosens. Bioelectron. 18 (5), 627–634.
Costa, L.A., Eiro, N., Fraile, M., Gonzalez, L.O., Saá, J., Garcia-Portabella, P., Vega, B., Schneider, J., Vizoso, F.J., 2021. Cell. Mol. Life Sci. 78 (2), 447–467.
Dagogo-Jack, I., Shaw, A.T., 2018. Nat. Rev. Clin. Oncol. 15 (2), 81–94.
Fleischer, S., Jahnke, H.-G., Fritsche, E., Girard, M., Robitzki, A.A., 2019. Biosens. Bioelectron. 126, 624–631.
Froehlich, K., Haeger, J.-D., Heger, J., Pastuschek, J., Photini, S.M., Yan, Y., Lupp, A., Pfarrer, C., Mrowka, R., Schleußner, E., Markert, U.R., Schmidt, A., 2016. J. Mammary Gland Biol. Neoplasia 21 (3), 89–98.
Gerasimenko, T., Nikulin, S., Zakharova, G., Poloznikov, A., Petrov, V., Baranova, A., Tonevitsky, A., 2020. Front. Bioeng. Biotechnol. 7 (474).
Gos lvez, M.A., Nieminen, R.M., 2003. New J. Phys. 5, 100, 100.
Gottmann, J., Hermans, M., Repiev, N., Ortmann, J., 2017. Micromachines 8 (4), 110.
Heaster, T.M., Landman, B.A., Skala, M.C., 2019. Front. Oncol. 9 (1144).
Hermans, M., 2014. Selective, Laser-Induced Etching of Fused Silica at High Scan-Speeds Using KOH. Japan Laser Processing Society, pp. 126–131.
Hof, L., Moreth, T., Koch, M., Liebisch, T., Kurtz, M., Tarnick, J., Lissek, S.M., Verstegen, M.M.A., van der Laan, L.J.W., Huch, M., Matthäus, F., Stelzer, E.H.K., Pampaloni, F., 2021. BMC Biol. 19 (1), 37.
Huang, Z., Yu, P., Tang, J., 2020. OncoTargets Ther. 13, 5395–5405.
Jahnke, H.G., Mewes, A., Zitzmann, F.D., Schmidt, S., Azendorf, R., Robitzki, A.A., 2019. Sci. Rep. 9 (1), 13875.
Jahnke, H.G., Poenick, S., Maschke, J., Kendler, M., Simon, J.C., Robitzki, A.A., 2014. Cancer Res. 74 (22), 6408–6418.
Jin, J.-Y., Yoo, S., Bae, J.-S., Kim, Y.-K., 2013. J. Micromech. Microeng. 24 (1), 015003.
Kim, S., Kim, J., Joung, Y.-H., Ahn, S., Choi, J., Koo, C., 2019. Micro. and Nano Sys. Lett. 7 (1), 15.
Kloss, D., Fischer, M., Rothermel, A., Simon, J.C., Robitzki, A.A., 2008. Lab Chip 8 (6), 879–884.
Kloß, D., Kurz, R., Jahnke, H.G., Fischer, M., Rothermel, A., Anderegg, U., Simon, J.C., Robitzki, A.A., 2008. Biosens. Bioelectron. 23 (10), 1473–1480.
Li, Y.-C.E., Lee, I.-C., 2020. Biosensors 10 (8), 88.
Lopez, C.M., Chun, H.S., Wang, S., Berti, L., Putzeys, J., Bulcke, C.V.D., Weijers, J.W., Firrincieli, A., Reumers, V., Braeken, D., Helleputte, N.V., 2018. IEEE J. Solid State Circ. 53 (11), 3076–3086.
Nii, T., Makino, K., Tabata, Y., 2020. Cancers 12 (10), 2754.
Pan, Y., Jiang, D., Gu, C., Qiu, Y., Wan, H., Wang, P., 2020. Microsys. Nanoeng. 6 (1), 23.
Schmid, Y.R.F., Bürgel, S.C., Misun, P.M., Hierlemann, A., Frey, O., 2016. ACS Sens. 1 (8), 1028–1035.
Seidel, D., Obendorf, J., Englich, B., Jahnke, H.G., Semkova, V., Haupt, S., Girard, M., Peschanski, M., Brustle, O., Robitzki, A.A., 2016. Biosens. Bioelectron. 86, 277–286.
Seidel, D., Rothe, R., Kirsten, M., Jahnke, H.G., Dumann, K., Ziemer, M., Simon, J.C., Robitzki, A.A., 2019. Biosens. Bioelectron. 123, 185–194.
Szulcek, R., Bogaard, H.J., van Nieuw Amerongen, G.P., 2014. JoVE: JoVE 85.
Zhang, Y., Zhang, X., Fang, J., Jiang, S., Zhang, Y., Gu, D., Nelson, R.D., LaRue, J.C., 2010. Application of SU-8 as the insulator toward a novel planar microelectrode array for extracellular neural recording. 2010. In: IEEE 5th International Conference on Nano/Micro Engineered and Molecular Systems, pp. 395–398.